2019 Rock Dynamics Summit– Aydan et al. (eds)
© 2019 Taylor & Francis Group, London, ISBN 978-0-367-34783-3

Numerical simulations on the seismic stability of rock foundations under critical facilities via dynamic nonlinear analysis

M. Ishimaru, A. Sekiguchi, & T. Okada
Central Research Institute of Electric Power Industry, Chiba, Japan

H. Morozumi
Kansai Electric Power Company, Inc., Osaka, Japan

ABSTRACT: Evaluation of seismic stability of critical facilities to earthquake-induced failure of rock foundations based on ground displacement is considered to be crucial. In this study, a constitutive model was developed to consider the effects of both shear and tensile failure of rock on the stress–strain relation derived from the multiple shear spring model. This model was then used for dynamic nonlinear analysis that considers progressive failure. The applicability of this analysis method to a dynamic centrifugal model test of a rock foundation was evaluated. The amounts of residual displacements of the analysis results were comparatively close to the model test results although the vibration step, which begins after the occurrence of residual displacements, was slightly faster than that of the model test.

1 INTRODUCTION

The occurrence of fatal, large-magnitude earthquakes in the recent past has led to increased attention on earthquake ground motion during the design phase of modern structures. Accordingly, quantitative assessment of seismic resistance of critical facilities to earthquake-induced failure of rock foundations has become important.

In Japan, the seismic stability of rock foundations has conventionally been evaluated in terms of their bearing capacity, inclination, and sliding (JEAG 4601-1987 1987). In terms of the sliding motion during an earthquake, a slip safety factor based on an equivalent linear analysis is conventionally used to evaluate the stability of rock foundations. However, a slip safety factor value of less than 1 does not necessarily indicate immediate ground instability (Ishimaru et al. 2018a). Therefore, the evaluation of seismic stability based on ground displacement is considered to be a more effective approach.

In this study, therefore, the applicability of a nonlinear analysis method that considers progressive failure to evaluate the seismic stability of rock foundations (including post-earthquake residual displacement) was investigated. This paper explains the proposed nonlinear analysis method. The applicability of this nonlinear analysis method to a dynamic centrifugal model test of rock foundation is presented.

2 NONLINEAR ANALYSIS METHOD

The influences of rock shear failure and tensile failure need to be properly considered in a nonlinear analysis. Ishimaru et al. (2018b) proposed a constitutive model of materials that considers strain-softening characteristics after shear failure in the shear stress–shear strain relation derived from the multiple shear spring model (Towhata & Ishihara 1985) in the two-dimensional plane strain state. In this study, modeling of the strength characteristics after tensile failure was added to the above constitutive model, and the method of redistribution of stress after tensile failure was modified.

In addition, the multiple shear spring model can consider anisotropy if different values of hardness and strength are assigned for each spring. However, the process becomes very complicated in dynamic analysis, and thus, isotropy was assumed in this study.

2.1 *Constitutive model of materials before failure*

The shear stress–shear strain curve before rock failure was modeled with the general hyperbolic equation (GHE) model (Tatsuoka & Shibuya 1992), which is given in Equation 1. The GHE model can be fitted to experimental results over a wide strain range.

$$\tau = \frac{G_0 \cdot \gamma}{\dfrac{1}{C_1(\gamma)} + \dfrac{1}{C_2(\gamma)} \cdot \dfrac{|\gamma|}{\gamma_r}} \tag{1}$$

Here, τ is the shear stress, γ is the shear strain, G_0 is the initial shear modulus, γ_r is the reference shear strain ($\gamma_r=\tau_{a0}/G_0$), and τ_{a0} is the initial reference shear strength. $C_1(\gamma)$ and $C_2(\gamma)$ are correction coefficients expressed as follows:

$$C_1(\gamma)=\frac{C_1(0)+C_1(\infty)}{2}+ \tag{2a}$$
$$\frac{C_1(0)+C_1(\infty)}{2}\cdot\cos\left\{\frac{\pi}{\alpha/(|\gamma|/\gamma_r)+1}\right\}$$

$$C_2(\gamma)=\frac{C_2(0)+C_2(\infty)}{2}+ \tag{2b}$$
$$\frac{C_2(0)+C_2(\infty)}{2}\cdot\cos\left\{\frac{\pi}{\beta/(|\gamma|/\gamma_r)+1}\right\}$$

where $C_1(0)$, $C_2(0)$, $C_1(\infty)$, $C_2(\infty)$, α, and β are parameters. The damping characteristics are assumed to follow the model given in Eq. 3, which uses a virtual shear stress–shear strain curve (Ishihara et al. 1985) and the maximum damping constant h_{max}.

$$h=h_{max}\cdot\left(1-G_R/G_0\right)^{\beta_1} \tag{3}$$

Here, G_R is the shear modulus at the strain level of the unloading point, and β_1 is the adjustment parameter of the damping characteristics. The method proposed by Ozutsumi & Iai (2001) is used to set the damping constant in the multiple shear spring model.

2.2 *Definitions of failure*

The shear strength is defined in Eq. 4 (in this paper, the compression side is defined as being positive):

$$\tau_f=c_p\cdot\cos\phi_p+\frac{\sigma_1+\sigma_3}{2}.\sin\phi_p \tag{4}$$

where τ_f is the peak shear strength, and c_p is the peak cohesion. In addition, ϕ_p is the peak internal friction angle, σ_1 is the maximum principal stress, and σ_3 is the minimum principal stress. Shear failure is estimated according to Eq. 5, and tensile failure is estimated according to Eq. 6, where σ_t is the tensile strength.

$$\left(\sigma_1-\sigma_3\right)/2\geq\tau_f \tag{5}$$

$$\sigma_3\leq\sigma_t \tag{6}$$

2.3 *Modeling after failure*

The shear stress–shear strain curve after rock failure also employs the GHE model shown in Eq. 1. However, the reference shear strain $\gamma_r=\tau_a/G_0$, and the reference shear strength τ_a decreases from the initial value τ_{a0} to the residual shear strength τ_r (Eq. 7) after rock failure.

$$\tau_r=a\cdot\left(\frac{\sigma_1+\sigma_3}{2}\right)^b \tag{7}$$

Here, a and b are the adjustment parameters of the residual shear strength. In addition, the damping characteristics after failure are assumed to be the same as those in Eq. 3.

Modeling of the reference shear strength τ_a and tensile strength σ_t after rock failure are explained below. Anisotropy should be considered for modeling the strength after rock failure, but the process becomes very complicated in dynamic analysis. Thus, we assume isotropy here. First, for tensile failure, we consider reducing the strength uniformly in all directions according to the number of tensile failure surfaces. More specifically, the analysis element is divided at a certain angle (N: division number), and the number of divided regions, including the tensile failure surface defined by the direction of the principal stress surface, is counted. Then, τ_a and σ_t are gradually reduced by Eqs. (8) and (9).

$$\tau_a=\tau_{as}\cdot\left(1-n_f/N\right)^{\alpha_1}+\tau_r\cdot\left\{1-\left(1-n_f/N\right)^{\alpha_1}\right\} \tag{8}$$

$$\sigma_t=\sigma_{ts}\cdot\left(1-n_f/N\right)^{\alpha_1} \tag{9}$$

where n_f is the number of divided regions including the tensile failure surface, α_1 is the adjustment parameter of the strength reduction, and τ_{as} and σ_{as} are the reference shear strength and tensile strength considering the influence of shear failure. τ_{as} and σ_{as} are gradually reduced by the following equations according to the amount of strain generated after shear failure, considering the gradient of strain softening.

$$\tau_{as}=\tau_r+\frac{\left(\tau_{a0}-\tau_r\right)}{\left(A\cdot\gamma^p+1\right)} \tag{10}$$

$$\sigma_{ts}=\frac{\sigma_{t0}}{\left(A\cdot\gamma^p+1\right)} \tag{11}$$

Here, σ_{t0} is the initial tensile strength, γ^p is the maximum value of the maximum shear strain (incremental amount from the value at failure), and A is the strain softening coefficient, which is a parameter that determines the rate of decrease in τ_{as} and σ_a.

2.4 *Redistribution of stress*

The method of redistribution of stresses exceeding strengths is as follows:

i. For shear failure, shrink the Mole's stress circle under the condition of fixed average principal stress.
ii. For tensile failure, shrink the Mole's stress circle under the condition of fixed maximum principal stress. If it exceeds the shear strength even after this treatment, shrink the Mole's stress circle

under the condition of fixed minimum principal stress.

iii. Apply residual force calculated from external force and stress.

3 DYNAMIC CENTRIFUGAL MODEL TEST

A dynamic centrifugal model test was performed to assess the seismic stability of rock foundations (Ishimaru et al. 2018a). The rock foundation model with a reduction ratio of 1:50 was constructed with artificial rock material and a weak layer. Vibration tests were performed in a centrifugal force field under a centrifugal acceleration of 50 g.

3.1 *Rock foundation model*

The rock foundation model and instrument arrangement are shown in Figure 1. The model was 200 mm (10 m upon real-scale conversion) in height and 300 mm in depth. The boundary surfaces had cutouts measuring 100 mm × 100 mm to avoid interference with the rigid box. The building model dimensions were 60 mm (width) × 40 mm (height) (3 m × 2 m upon real-scale conversion), and the density of the building material was 1200 kg/m^3. In addition, the bottom of the building model and ground surface were fixed with an adhesive.

The measured variables included accelerations produced under and on the ground surface along with the corresponding displacements induced in the building model and on the ground surface.

3.2 *Properties of the rock foundation model*

The rock foundation model was created from cement-modified soil with a curing period of 7 d. For a soil volume of approximately 1 m^3, the formulation comprised 82 kg of high early-strength Portland cement, 370 kg of distilled water, 817 kg of crushed limestone sand, 817 kg of fine limestone powder, and 1 kg of admixture. Table 1 lists the physical properties of the artificial rock materials. The properties were obtained from various physical and mechanical tests. Figure 2 shows the dynamic deformation characteristics obtained from cyclic triaxial tests.

Based on the work by Ishimaru & Kawai (2011), the weak layer within the rock mass was reproduced by installing a 0.2 mm thick Teflon sheet within the rock foundation model before the artificial rock material started hardening. The resultant artificial weak layer had constant degrees of roughness, bite, etc. Prior examination confirmed that the cohesion between the post-hardening artificial rock material and Teflon sheet was very small. Under this condition, the shear resistance of the artificial weak layer can be considered to be equal to the frictional force generated between the artificial rock material and Teflon sheet. Therefore, the frictional force generated between the artificial rock material and Teflon sheet under normal-stress loading was examined through a single-plane shearing test. Table 1 shows the maximum and residual shear resistances increased in proportion to the normal stress.

Table 1. Physical properties of the artificial rock materials and weak layer (σ_m: mean stress).

	Rock	Weak layer
Unit weight	20.3 kN/m^3	20.6 kN/m^3
Peak shear strength	c_p = 267.1 kN/m^2 φ_p = 34.7°	c_p = 0.0 kN/m^2 φ_p = 28.6°
Residual shear strength	a = 4.61, b = 0.70 ($\tau_r = a \times \sigma_m{}^b$)	c_r = 0.0 kN/m^2 φ_r = 19.3°
Tensile strength	σ_t = 41.4 kN/m^2	σ_t = 0.0 kN/m^2
Initial elastic shear modulus	933000 kN/m^2	2800 kN/m^2
Poisson's ratio	0.42	0.49

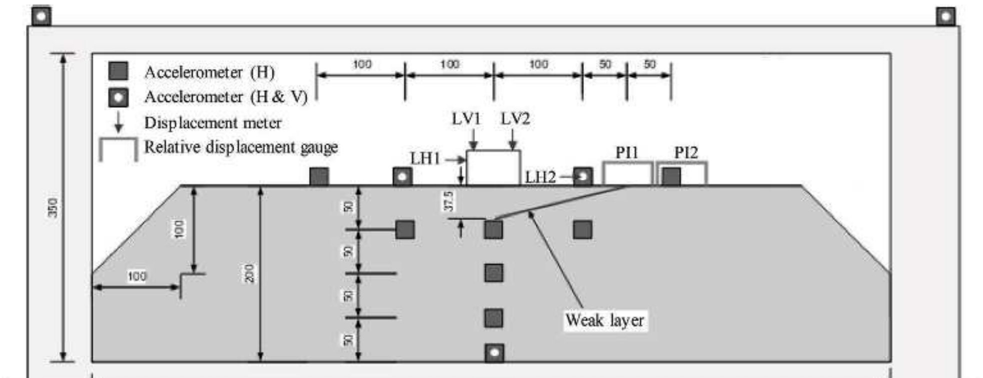

Figure 1. Rock foundation model and instrument arrangement (units: mm).

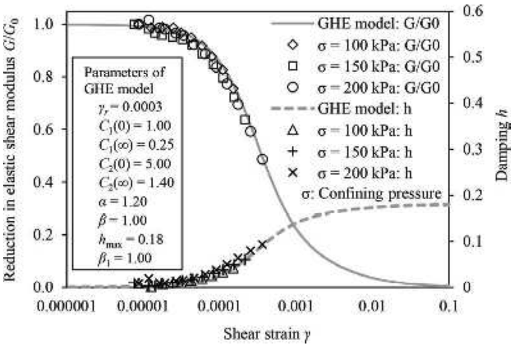

Figure 2. Dynamic deformation characteristics of the artificial rock material obtained from cyclic triaxial tests.

Table 2. Maximum values of the acceleration amplitude at different vibration steps (real-scale conversion).

Vibration step	Frequency	Horizontal acc. m/s^2	Vertical acc. m/s^2
d01	1.2	0.57	0.13
d02	1.2	3.47	0.42
d03	1.2	5.72	1.15
d04	1.2	7.77	0.91
d05	1.2	9.16	1.22
d06	1.2	10.40	1.50
d07	1.6	8.68	1.87
d08	1.6	10.04	2.88
d09	1.6	11.53	3.84
d10	1.6	11.25	3.39

3.3 *Input acceleration*

The input acceleration was provided in the form of a sinusoidal wave with a wavenumber of 20 (frequencies of 1.2 and 1.6 Hz upon real-scale conversion) in the main part with four tapers before and after that. During the test, the acceleration amplitude was increased for each vibration step. A horizontal movement was the only input. However, the vertical motion, which was considered to be caused by the rocking of the shaking table, was also measured during vibration. Figure 3 shows the input acceleration of vibration step d04, and Table 2 lists the maximum acceleration amplitudes at different vibration steps. The 1.6 Hz excitation produced a greater vertical motion than the 1.2 Hz excitation owing to the characteristics of the experimental apparatus.

3.4 *Test results*

Figure 4 shows the accumulated residual values of the horizontal displacements of the building model and ground at different vibration steps. This figure confirms that the residual displacements rapidly increased after vibration step d09.

Figure 5 shows the strain distribution calculated from images captured by a high-speed camera at vibration step d10. Cracks connecting the lower end of the weak layer and the left side of the building model were generated, although they were not yet clear in images captured at vibration step d09. Owing to the occurrence of these cracks, the upper part of the weak layer was considered to have moved.

4 NUMERICAL SIMULATIONS

4.1 *Analysis conditions*

The set values for the parameters of the artificial rock materials used for the nonlinear analyses are listed in Table 3.

The other parameters were set according to the results of the physical and mechanical tests

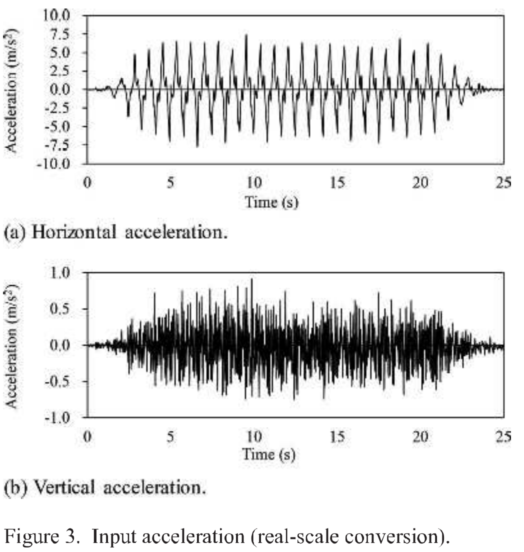

Figure 3. Input acceleration (real-scale conversion).

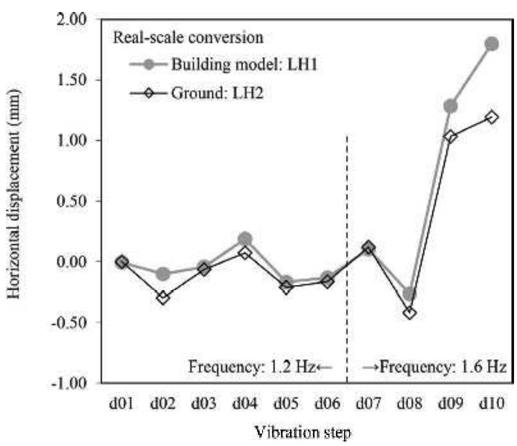

Figure 4. Accumulated residual values for the horizontal displacements of the building model and ground at different vibration steps.

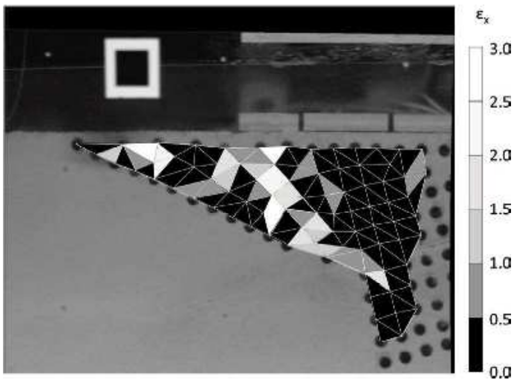

Figure 5. Horizontal strain distribution calculated from images taken with a high-speed camera at vibration step d10.

Table 3. Setting parameters of the constitutive model.

	Case 1	Case 2	Case 3
Number of multiple shear springs in the semicircle		12	
Parameters of strength reduction after tensile failure: N, α_1	$N = 18$, $\alpha_1 = 0.5$	$N = 18$, $\alpha_1 = 0.25$	$N = 18$, $\alpha_1 = 0.125$
Strain softening coefficient A		$A = 300$	

(Table 1 and Figure 2). The strain softening coefficient A was obtained from the relation of the deviator stress σ_d minus the axial strain ε_a in the strain-softening process after the peak of the plane strain compression tests. In addition, case studies were conducted on the parameters N and α_1 related to the strength reduction after tensile failure occurred.

In contrast, the artificial weak layer was modeled to joint elements. The unit weight of the artificial weak layer was 20.6 kN/m^3, which was equal to that of the Teflon sheet, and the corresponding Poisson's ratio was 0.49 based on the assumption of no volume change. The pseudo shear modulus of elasticity, which was induced by modeling the artificial weak layer as joint elements, was set as 2800 kN/m^2 from the gradient up to the maximum shear resistance during the single-plane shearing tests.

For the boundary conditions in the numerical simulations of the model test, the bottom was fixed, and the joint elements (tension/shear spring: 0 kPa; compression spring: 1.0×10^8 kPa) were installed on the side. A self-weight analysis was performed by dividing the value of gravity by 100. The accelerations of the shaking table were then input for the earthquake response analyses. In the seismic response analyses, the stress and deformation state of the preceding step were carried to the next step considering 1 % stiffness-proportional damping at 10 Hz. In addition, the time increment of the calculation was 2.0×10^{-4} s, and the convergence criterion was set to a residual force norm/external force norm of less than 1.0×10^{-4}. The iterative calculation reached 10x, and residual forces were carried over to the next calculation step.

4.2 *Analysis results*

Figure 6 shows the accumulated residual values for the inclination of the building model at different vibration steps. This figure confirms that the inclination amounts of the analysis results are smaller than those of the model test although the inclination amounts of the analyses rapidly increase at vibration step d08. This may be due to properties of the joint element for the artificial weak layer. In particular, the vertical rigidity of the joint element will be examined in detail.

Figure 7 and Figure 8 show the accumulated residual values of the horizontal displacements of the building model and ground at different vibration steps, respectively. These figures confirm that the faster the strength reduction after tensile failure, the larger the amount of residual displacements. However, the difference between Case 2 and Case 3 is small, and the amounts of residual displacements were comparatively close to the model test results although the vibration step, which begins after the occurrence of residual displacements, was slightly faster than that of the model test.

Figure 9 shows the tensile failure surface ratio n_f/N at the end of vibration step d08 for Case 2. This figure confirms that the tensile failures connecting the lower end of the weak layer and the left side of the building model were generated as the same of the model test result shown in Figure 5.

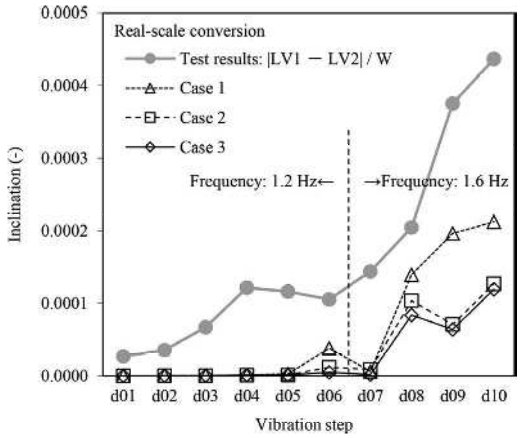

Figure 6. Accumulated residual values for the inclination of the building model at different vibration steps.

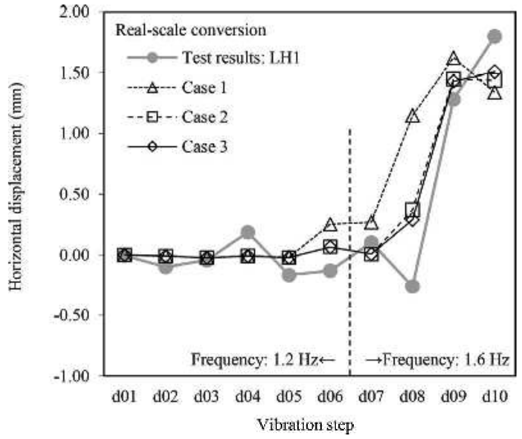

Figure 7. Accumulated residual values for the horizontal displacements of the building model at different vibration steps.

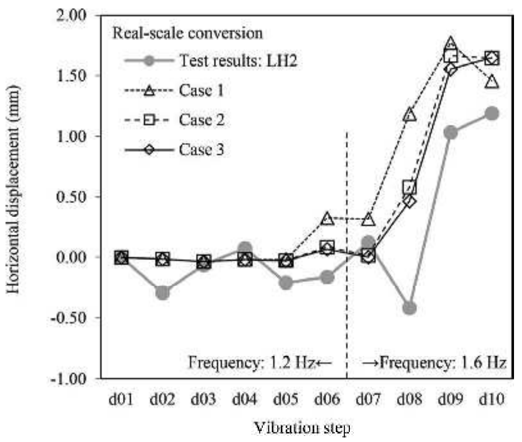

Figure 8. Accumulated residual values for the horizontal displacements of the ground at different vibration steps.

5 CONCLUSION

This study developed a constitutive model that considers the effects of both shear and tensile failure of rock on the stress–strain relation derived from the multiple shear spring model. This model was then used for dynamic nonlinear analysis that considers progressive failure.

The applicability of this analysis method to a dynamic centrifugal model test was evaluated. The vibration step, which begins after the occurrence of residual displacements, was slightly faster than that of the model test although the amounts of residual displacements were comparatively close to the model test results. This may be because

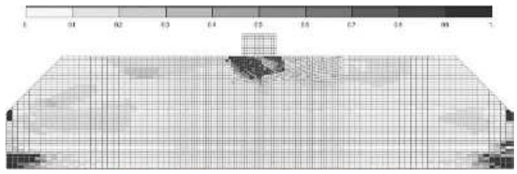

Figure 9. Tensile failure surface ratio at the end of vibration step d08 for Case 2.

anisotropy was not considered in this analysis. To evaluate the displacement more quantitatively, the proposed method needs to consider anisotropy, such as changes in strength and rigidity according to the failure surface direction.

Another problem concerns setting the parameters related to the strength reduction after tensile failure. Conservative evaluation is possible if large values are set. However, for a more accurate quantitative evaluation of the amount of displacement, a detailed examination for setting the parameters is necessary.

REFERENCES

Ishihara, K., Yoshida, N. and Tsujino, S. 1985. Modeling of stress-strain relations of soils in cyclic loading. *Proc. 5th Int. Conf. Numerical Methods in Geomechanics, Nagoya*, Vol. 1: 373–380.

Ishimaru, M., Hashi, K., Oikawa, K. and Kawai, T. 2018b. Nonlinear Analysis Method for Evaluating the Seismic Stability of Rock Slopes Considering Progressive Failure, *Journal of Earthquake and Tsunami*, Vol. 12, No. 4: 1–16.

Ishimaru, M. and Kawai, T. 2011. Centrifuge model test on earthquake-induced failure behaviour of slope in discontinuous rock mass. *Proc. 12th Int. Congress on Rock Mechanics, Beijing*, 1919–1922.

Ishimaru, M., Sekiguchi A., Okada, T., Hiraga, K. and Ozawa, K. 2018a. Experimental study on seismic stability of foundation rocks under critical facilities, *Rock Dynamics - Experiments, Theories and Applications; Proc. 3rd Int. Conf. on Rock Dynamics and Applications, Trondheim*, 569–574.

JEAG 4601-1987. 1987. Technical Guidelines for Aseismic Design of Nuclear Power Plants, Japan.

Ozutsumi, O. and Iai, S. 2001. Adjustment method of the hysteresis damping for multiple shear spring model. *Proc. 4th Int. Conf. Recent Advances in Geotechnical Earthquake Engineering and Soil Dynamics, San Diego, California*, Paper No. 1.68: 1–6.

Tatsuoka, F. and Shibuya, S. 1992. Deformation characteristics of soils and rocks from field and laboratory tests. *Proc. 9th Asian Regional Conf. Soil Mechanics and Foundation Engineering, Bangkok*, Vol. 2: 101–170.

Towhata, I. and Ishihara, K. 1985. Modelling soil behavior under principal stress axes rotation. *Proc. 5th Int. Conf. Numerical Methods in Geomechanics, Nagoya*, Vol. 1: 523–530.